J Neurophysiol 107: 1032–1041, 2012.
First published November 30, 2011; doi:10.1152/jn.00453.2011.

Synaptic release and extracellular actions of Zn^{2+} limit propagation of spreading depression and related events in vitro and in vivo

Isamu Aiba,[1] Andrew P. Carlson,[2] Christian T. Sheline,[3] and C. William Shuttleworth[1]
Departments of [1]Neurosciences and [2]Neurosurgery, University of New Mexico, Albuquerque, New Mexico; and [3]Department of Ophthalmology and the Neuroscience Center of Excellence, Louisiana State University Health Sciences Center, New Orleans, Louisiana

Submitted 18 May 2011; accepted in final form 29 November 2011

Aiba I, Carlson AP, Sheline CT, Shuttleworth CW. Synaptic release and extracellular actions of Zn^{2+} limit propagation of spreading depression and related events in vitro and in vivo. *J Neurophysiol* 107: 1032–1041, 2012. First published November 30, 2011; doi:10.1152/jn.00453.2011.—Cortical spreading depression (CSD) is a consequence of a slowly propagating wave of neuronal and glial depolarization (spreading depolarization; SD). Massive release of glutamate contributes to SD propagation, and it was recently shown that Zn^{2+} is also released from synaptic vesicles during SD. The present study examined consequences of extracellular Zn^{2+} accumulation on the propagation of SD. SD mechanisms were studied first in murine brain slices, using focal KCl applications as stimuli and making electrical and optical recordings in hippocampal area CA1. Elevating extracellular Zn^{2+} concentrations with exogenous $ZnCl_2$ reduced SD propagation rates. Selective chelation of endogenous Zn^{2+} (using TPEN or CaEDTA) increased SD propagation rates, and these effects appeared due to chelation of Zn^{2+} derived from synaptic vesicles. Thus, in tissues where synaptic Zn^{2+} release was absent [knockout (KO) of vesicular Zn^{2+} transporter ZnT-3], SD propagation rates were increased, and no additional increase was observed following chelation of endogenous Zn^{2+} in these tissues. The role of synaptic Zn^{2+} was then examined on CSD in vivo. ZnT-3 KO animals had higher susceptibility to CSD than wild-type controls as evidenced by significantly higher propagation rates and frequencies. Studies of candidate mechanisms excluded changes in neuronal excitability, presynaptic release, and GABA receptors but left open a possible contribution of *N*-methyl-D-aspartate (NMDA) receptor inhibition. These results suggest the extracellular accumulation of synaptically released Zn^{2+} can serve as an intrinsic inhibitor to limit SD events. The inhibitory action of extracellular Zn^{2+} on SD may counteract to some extent the neurotoxic effects of intracellular Zn^{2+} accumulation in acute brain injury models.

cortical spreading depression; zinc; CA1; ZnT-3; NMDA-R

CORTICAL SPREADING DEPRESSION (CSD) was discovered as a slowly propagating suppression of electrocorticographic (ECoG) activity (Leão 1944) and subsequently characterized as a regenerative, severe depolarization of neurons and glia (Somjen 2001). CSD is thought to underlie aspects of migraine, and events very similar to CSD have recently been recorded with relatively high frequencies in patients with ischemic stroke, subarachnoid hemorrhage, traumatic brain injury, and intracerebral hemorrhage (Dreier 2011; Lauritzen et al. 2011). Because suppression of ECoG activity may not be readily apparent during propagation of these events in injured brain, the general term spreading depolarization (SD) has been used to emphasize the important underlying mechanism. Recovery from SD places a substantial metabolic burden on tissues, and it is very likely that failure of ionic homeostasis caused by repetitive SD events contributes to infarct enlargement in injured brain. Thus prevention of SD is considered a promising target for reducing the progression of acute brain injuries (Dreier 2011; Hartings et al. 2011; Lauritzen et al. 2011).

The propagation of SD is associated with increased extracellular glutamate concentrations (Fabricius et al. 1993), and activation of *N*-methyl-D-aspartate (NMDA)-type glutamate receptors (NMDA-Rs) contributes to SD progression in many experimental situations. Thus NMDA-R antagonists inhibit SD and related events both in vitro and in vivo (Anderson and Andrew 2002; Faria and Mody 2004; Gill et al. 1992; Hartings et al. 2003; Peeters et al. 2007). The divalent cation Zn^{2+} is enriched in synaptic vesicles at many glutamatergic synapses due to the activity of a specific transporter termed ZnT-3 (Cole et al. 1999). A range of studies have concluded that Zn^{2+} can be coreleased with glutamate following vesicle fusion at some synapses (Assaf and Chung 1984; Howell et al. 1984; Qian and Noebels 2005) and can potentially modify synaptic function by altering the activity of ion channels, receptors, and transporters (Frederickson et al. 2005). NMDA-Rs are among the most well-studied molecular targets for extracellular Zn^{2+} actions. Structural studies have identified high- and low-affinity Zn^{2+} binding sites in the NH_2 termini of NR2A and NR2B subunits, and interaction with Zn^{2+} causes suppression of channel activity in an allosteric manner (Gielen et al. 2009). In addition to allosteric inhibition, lower-sensitivity ($IC_{50} > 20\ \mu M$) voltage-dependent inhibition by Zn^{2+} has also been described (Paoletti et al. 1997). Because Zn^{2+} and glutamate are expected to be coreleased at synapses where NMDA-R are present, Zn^{2+} could potentially serve to limit excessive activation of NMDA-R in many forms of brain pathology (Paoletti et al. 2009). In addition to NMDA-Rs, Zn^{2+} has been shown to attenuate inhibitory synaptic transmission mediated by ionotropic GABA receptors, with substantially different sensitivities depending on subunit composition (Smart et al. 2004). These interactions could potentially lead to complex effects of Zn^{2+} on SD.

We recently reported that intracellular accumulation of Zn^{2+} contributed to initiation of some forms of SD in brain slices, including events generated by ischemia-like conditions (Dietz et al. 2008). In addition, SD propagation was shown to involve substantial release of vesicular Zn^{2+} into the extracellular space in a wavelike manner that accompanied the SD wave front (Carter et al. 2011). We found that Zn^{2+} from this source

Address for reprint requests and other correspondence: C. W. Shuttleworth, Dept. of Neurosciences, Univ. of New Mexico School of Medicine, Albuquerque, NM 87131-0001 (e-mail: bshuttleworth@salud.unm.edu).

accumulated postsynaptically and speculated that this intracellular accumulation may contribute to further SD initiation or possibly injury. However, in the current study, we tested whether extracellular Zn^{2+} accumulation during SD could also have a self-limiting effect on SD propagation. The current results show that extracellular Zn^{2+} does serve to limit SD propagation and suggest dual roles for Zn^{2+} in SD and injury progression.

MATERIALS AND METHODS

Animals. All experimental procedures using animals were reviewed and approved by the Institutional Animal Care and Use Committee of the University of New Mexico. For in vitro characterization of $ZnCl_2$ inhibitor and chelator effects, 4- to 10-wk-old mice (FVB/N or C57BL/6) of either sex were used, and drug effects were compared with control SD responses generated in the same slices. For in vitro studies of effects of ZnT-3 deletion, tissues from age-matched wild-type (WT) C57BL/6 animals and ZnT-3 knockout (KO) animals were compared. The ZnT-3 KO mice were originally generated as described previously (Cole et al. 1999) and back-crossed onto C57BL/6 for >13 generations. Experiments between genotypes were alternated. For in vivo CSD studies, 11- to 16-wk-old male animals were used, alternating between age-matched C57BL/6 and ZnT-3 KO.

Drugs. Unless otherwise stated, reagents were obtained from Sigma-Aldrich (St. Louis, MO). Histidine (200 μM) was included in all solutions used for $ZnCl_2$ studies (including for studies of control responses) to increase Zn^{2+} solubility in the phosphate-containing recording solutions (Rumschik et al. 2009).

Statistical analysis. All results are presented as means ± SE and were analyzed by Student's *t*-tests or one-way ANOVA with appropriate post hoc *t*-tests unless otherwise mentioned. Throughout the study, events >2 standard deviations from the mean were excluded as outliers.

In vitro SD recordings. Murine brain slices were prepared as previously described (Carter et al. 2011). Briefly, mice were deeply anesthetized and decapitated, and brains were extracted into ice-cold cutting solution. Coronal slices (350 μm) were prepared with a vibratome and transferred to artificial cerebrospinal fluid (ACSF). Brain slices were allowed to recover at 35°C for 1 h and then maintained in ACSF at room temperature until transferred to the recording chamber (RC-27 L; Warner Instruments). Slices were continuously superfused with ACSF (containing, in mM, 126 NaCl, 3 KCl, 1.25 NaH_2PO_4, 1 $MgSO_4$, 26 $NaHCO_3$, 2 $CaCl_2$, and 10 glucose, equilibrated with 95% O_2-5% CO_2) at 32°C.

SD was generated in the hippocampal CA1 region by localized microinjection of 1 M KCl from a conventional patch micropipette (tip diameter 10–20 μm) by using a pressure ejection controller (Parker PicoSpritzer III; General Valve; 40 psi). The stimulus threshold was determined by incrementally increasing pulse duration (10–100 ms), and all experiments were conducted using pulse durations 50–100% longer than the threshold (typically 50–150 ms). Drug challenges were compared with control responses generated in the same slices.

As a control for osmotic effects of KCl microinjection, we confirmed that local injection of equimolar NaCl (1 M) did not mimic the responses to localized KCl microinjections when tested in the same slices. Thus NaCl pulses did not generate propagating SD-like events, as determined from propagating light transmission increases, or direct current (DC) potential shifts at the recording site ($n = 3$).

SD propagation through the CA1 region was detected electrically and optically. DC potential shifts were recorded with extracellular electrodes (0.5–1 MΩ) placed in stratum radiatum 50 μm below the slice surface. Signals were amplified with a MultiClamp 700A amplifier and acquired using pCLAMP 9.2 software (Molecular Devices). Intrinsic optical signals were assessed from transmitted light from a halogen source (>575 nm) and collected by a charge-coupled device (CCD) camera (TILL Imago, controlled by TILLvisION v4.0 software; TILL Photonics). SD propagation rates were determined by tracking the wave front of intrinsic optical signals (IOS) following image acquisition at 0.33 Hz (Fig. 1*A*).

Slice electrophysiology. Single-cell recordings were obtained from hippocampal CA1 pyramidal neurons. Neurons were visually identified, and whole cell clamp was made with 1- to 2-MΩ glass pipettes. Intrinsic excitability and excitatory postsynaptic currents (EPSCs) were recorded with potassium gluconate-based internal solution (10 mM HEPES, 135 mM potassium gluconate, 8 mM NaCl, 1 mM $MgCl_2$, 2 mM ATP-Na_2, and 0.3 mM GTP-Na_3) in ACSF. Intrinsic excitability was examined by voltage responses to ±200-pA current pulses with no holding current applied. Prolonged recording (>10 min) often resulted in rundown of action potential frequency, and therefore intrinsic excitability was measured 2–3 min after establishment of whole cell configuration from neurons preexposed to $ZnCl_2$ for at least 10 min.

Field excitatory postsynaptic potentials (fEPSPs) were evoked by stimulation of Schaffer collateral inputs using a concentric bipolar electrode and detected using glass electrodes in the CA1 subfield. After input output curves were determined, stimulation intensity was set at ~50% maximal for subsequent pharmacological analysis. For isolation of NMDA-R components of fEPSPs ($fEPSP_{NMDA}$), slices were first incubated in low-magnesium ACSF [50 μM Mg^{2+} balanced with increased Ca^{2+} (3 mM)] for 20 min, and then 10 μM 6,7-dinitroquinoxaline-2,3-dione (DNQX) and 10 μM bicuculline were added.

Intracellular and extracellular imaging of FluoZin-3 fluorescence. Intracellular Zn^{2+} was measured from single CA1 neurons loaded with FluoZin-3 as described previously (Vander Jagt et al. 2009). Patch pipettes contained 10 mM HEPES, 135 mM potassium gluconate, 8 mM NaCl, 1 mM $MgCl_2$, 2 mM ATP-Na_2, 0.3 mM GTP-Na_3, and 500 μM FluoZin-3. Dialysis was strictly limited to 3 min, which restricted final intracellular indicator concentration to levels <100 μM. Electrodes were then slowly removed, and neurons were allowed to recover for 15 min. FluoZin-3 fluorescence was excited at 495 nm (80 ms, 0.2 Hz), and band-pass-filtered (535 ± 25 nm) emission fluorescence was collected with the CCD system. Neurons were exposed with either ZnPyr (1 μM Zn^{2+}, 100 nM pyrithione) or $ZnCl_2$ (100 μM) for 10 min and then washed with ACSF. FluoZin-3 signals were background-corrected using regions of interest from adjacent nonloaded neurons and expressed as the relative change in fluorescent intensity ($\Delta F/F_0$).

Extracellular Zn^{2+} accumulation was imaged as described previously (Carter et al. 2011). Slices were superfused with 1 μM FluoZin-3-containing ACSF. To enhance signal-to-noise ratio, 1 mM CaEDTA was included (Carter et al. 2011; Qian and Noebels 2005). FluoZin-3 signals were monitored with the CCD system at 1 Hz. To correct for autofluorescence changes, signals were background-subtracted using recordings made in the same slices but without FluoZin-3 addition.

In vivo CSD. Mice were anesthetized with isoflurane (3% induction, 1–1.25% maintenance) and nitrous oxide (70%) in oxygen (30%) and positioned in a stereotaxic frame. The depth of anesthesia was monitored throughout the experiments, and the isoflurane concentration was adjusted to maintain depth sufficient to prevent reflex responses. The scalp was opened, anterior and posterior burr holes were made ~1 mm apart bilaterally in the parietal bone, and the distance between them was measured for calculation of CSD propagation rates. Craniotomies anterior to the burr holes were made for either electrical or KCl stimulation (see Fig. 4*A*). When windows were not used for experiments, saline-filled cotton pads were set on the brain surface. In all experiments, glass electrodes were placed through ipsilateral burr holes, ~300 μm below the cortical surface, and electrical activity was amplified by using an Axoprobe 1A amplifier (Axon Instruments) and digitized with a PowerLab 8/16 system (ADInstruments). The digital data were segregated and filtered via alternating current and DC coupling for ECoG and extracellular DC recording, respectively. CSD propagation rates were calculated from

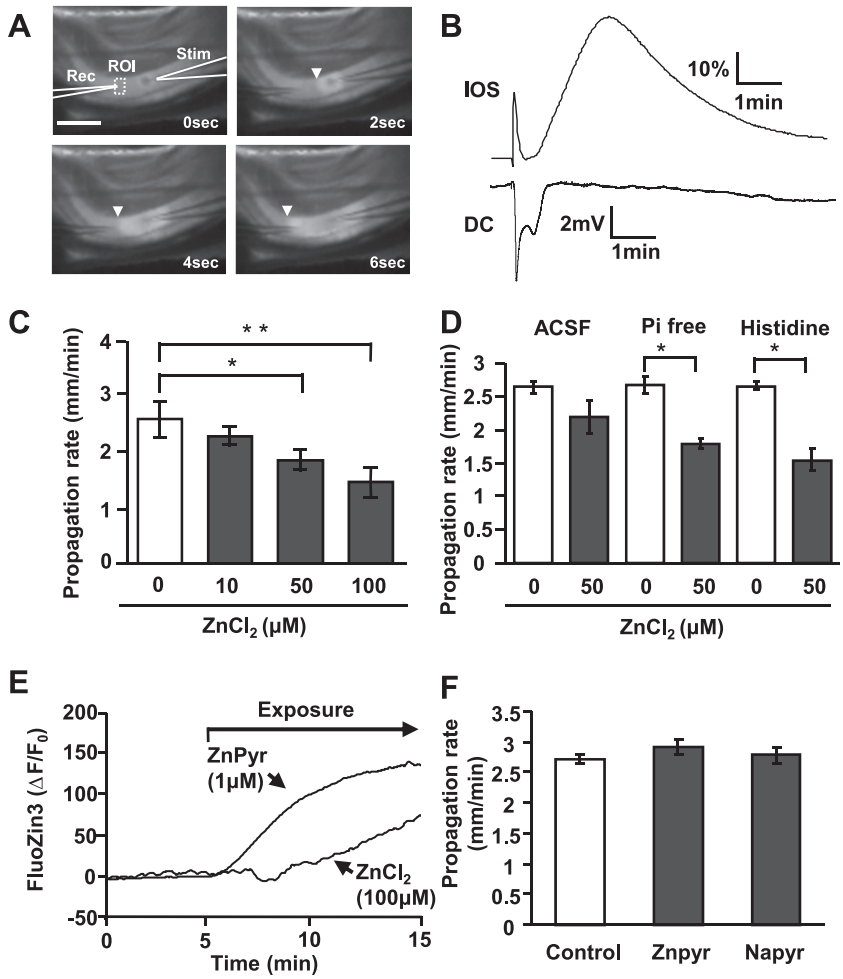

Fig. 1. Extracellular Zn^{2+} inhibits spreading depolarization (SD) propagation. *A*: images showing electrode placement and propagation of SD through the hippocampal CA1 subregion. SD was generated by local microinjection of KCl (10-ms pulse) from a stimulation pipette (Stim) and detected using an extracellular recording electrode (Rec). SD was also tracked from propagating intrinsic optical signal (IOS) increases (>575-nm transmission; arrowheads). Scale bar = 250 μm. ROI, region of interest. *B*: time courses of IOS and electrical [direct current (DC)] signals generated from the preparation illustrated in *A*. *C*: brief $ZnCl_2$ preexposures [10 min in histidine-supplemented artificial cerebrospinal fluid (ACSF)] resulted in concentration-dependent reductions in SD propagation rate (*$P < 0.05$, **$P < 0.01$; $n = 5$). *D*: comparison of buffer composition on effectiveness of $ZnCl_2$ applications. $ZnCl_2$ (50 μM; 10 min) was more effective in phosphate-free ACSF (P_i-free) and histidine-supplemented ACSF (200 μM histidine) than in control ACSF (*$P < 0.05$; $n = 5$). *E*: intracellular Zn^{2+} accumulation assessed in single neurons loaded with FluoZin-3. $ZnCl_2$ exposures (100 μM) resulted in slow intracellular accumulation, and more rapid increases were observed with ZnPyr (1 μM $ZnCl_2$ with 100 nM pyrithione). $\Delta F/F_0$, relative change in fluorescent intensity. *F*: preferentially loading intracellular Zn^{2+} had no effect on SD propagation rate. Exposure to ZnPyr (as in *E*, followed by brief wash) did not reduce SD propagation rate, and no effects were observed with a control for nonspecific effects of pyrithione (sodium pyrithione, NaPyr; 100 nM; $n = 5$).

the latency of CSD and the measured distance between the recording electrodes.

Durations of ECoG suppression were calculated after CSD elicited by bipolar electrical stimulation. CSD propagation rates and frequencies were calculated from repetitive CSDs generated by KCl applications. A gelatin sponge (Gelfoam; Ethicon 360) soaked with 0.3 M KCl was used to apply KCl on the anterior cranial widow, and electrical responses were recorded for 30 min. During the 30-min trial, KCl was reapplied to prevent drying either immediately after detection of each SD event or after 10 min in the absence of significant electrical responses. To be included in the analysis, events must have propagated in an anterior-to-posterior direction with <50% decreased in amplitude between electrodes. Repetitive SDs were tested in both hemispheres, and the data from each animal were averaged.

After completion of the study, mice were euthanized by intraperitoneal injection of a barbiturate overdose.

RESULTS

Extracellular Zn^{2+} inhibits SD propagation. We first examined the effects of elevating extracellular Zn^{2+} on the propagation of SD events generated in brain slice preparations. SD was triggered by brief microinjection of KCl into stratum radiatum of area CA1, and SD was detected by a combination of optical (IOS) and extracellular DC recording (see MATERIALS AND METHODS). The experimental setup and representative recordings are shown in Fig. 1, *A* and *B*. Under control conditions, SD was visualized as a wave of increased light transmittance that propagated at ~2.5 mm/min in both directions from the site of KCl application. Opposite to optical responses to KCl, local microinjection of NaCl caused localized nonpropagating decrease of light transmission, likely due to tissue constriction following increased osmolarity (data not shown). A biphasic DC potential shift characteristic of SD was recorded coincident with arrival of the optical signal at the extracellular recording electrode site (Fig. 1*B*). These baseline responses are consistent with a large body of prior literature of SD in hippocampal slices (Somjen 2001).

The effects of elevating extracellular Zn^{2+} concentrations were tested following bath application of $ZnCl_2$. For all experiments testing effects of exogenous $ZnCl_2$, 200 μM histidine was included in recording solutions to increase its solubility in phosphate-containing solutions (Rumschik et al. 2009). Histidine alone had no significant effect on SD propagation (Fig. 1*D*, discussed below) and was included in control and test recording solutions for all studies involving $ZnCl_2$. $ZnCl_2$ exposures were kept brief (10 min) to maximize the contribution of effects on extracellular sites and reduce possible intracellular accumulation. Under these conditions, the propagation rates of SD were concentration-dependently decreased by Zn^{2+}, with significant inhibitory effects at 50 and 100 μM (Fig. 1*C*). The observed Zn^{2+} effect was completely reversed by brief coincubation with the membrane impermeable Zn^{2+} chelator CaEDTA (1 mM, 10 min, $n = 5$).

The suitability of this approach with histidine supplementation to increase availability of Zn^{2+} in ACSF was confirmed in a set of pilot studies comparing $ZnCl_2$ additions in *1*) normal ACSF, *2*) ACSF supplemented with histidine, and *3*) modified ACSF lacking added phosphates. Without $ZnCl_2$ additions, SD propagation in all three solutions were identical ($P > 0.05$). When 100 μM $ZnCl_2$ was applied in normal ACSF, there was an obvious visible precipitate likely due to formation of zinc-phosphate complexes. This was not observed in histidine or phosphate-free solutions. Further comparisons between the three solutions were therefore made using 50 μM $ZnCl_2$. Figure 1*D* shows that this concentration caused similar inhibition of SD propagation rate effective in both P_i-free and histidine solutions (P_i-free 33.6 ± 0.01%, histidine 42.0 ± 0.05%) but significantly less effective in ACSF (17.3 ± 0.09%; $P < 0.01$ compared with P_i-free and histidine; $n = 5$), consistent with greater extracellular availability (Fig. 1*D*). Superfusion in phosphate-free solution often led to significant tissue swelling (as assessed by light-transmission increases), and thus to avoid potential effect of phosphate removal on cellular metabolism, we chose histidine supplementation rather than phosphate-free ACSF for the remaining studies (Rumschik et al. 2009).

Single-cell Zn^{2+} imaging (following intracellular FluoZin-3 loading; see MATERIALS AND METHODS) revealed relatively slow but significant intracellular Zn^{2+} accumulation following brief exposures to $ZnCl_2$ (100 μM $ZnCl_2$, 48.7 ± 10.0% $\Delta F/F_0$ increase after 10-min exposure, $n = 3$; Fig. 1*E*). Because intracellular Zn^{2+} accumulation is known to modulate neuronal excitability (Frederickson et al. 2005), we next tested whether intracellular accumulation of Zn^{2+} could contribute to inhibition of SD propagation. An approach to increase intracellular Zn^{2+} loading selectively was carried out by exposure of slices to a low concentration of a Zn^{2+}-ionophore complex (ZnPyr for 10 min) and followed by brief wash (3 min) to minimize extracellular Zn^{2+} levels. This Zn^{2+} loading protocol resulted in rapid intracellular Zn^{2+} accumulation that reached significantly higher levels than observed with the $ZnCl_2$ exposures (Fig. 1*E*; 1 μM ZnPyr: 123.8 ± 12.5% after 10-min loading and 3-min wash; $P < 0.01$ vs. 100 μM $ZnCl_2$, 10 min, *t*-test; $n = 3$). Figure 1*F* shows that preferentially increasing intracellular Zn^{2+} loading with ZnPyr did not have any effect on SD propagation rate.

As a control, we evaluated other effects of pyrithione. Pyrithione itself is a membrane permeable chelator, and it is possible that presence of pyrithione depleted synaptic vesicle Zn^{2+} pools and thereby modulated SD propagation. The content of the available synaptic vesicle Zn^{2+} pool was analyzed by recording extracellular Zn^{2+} accumulation during SD, utilizing extracellular FluoZin-3 (Carter et al. 2011). Exposure to sodium pyrithione (NaPyr; 100 nM, 15 min) did not significantly reduce extracellular Zn^{2+} transients attributed to release from synaptic vesicles (control 111.4 ± 23.9% vs. NaPyr 105.1 ± 15.7%, peak $\Delta F/F_0$; $P = 0.84$; $n = 3$). Consistent with these results, NaPyr did not affect SD propagation rate (Fig. 1*F*, NaPyr).

Taken together, these results imply that extracellular rather than intracellular actions of Zn^{2+} most likely explain the inhibitory effects of $ZnCl_2$ on SD shown in Fig. 1*C*.

Vesicular Zn^{2+} limits SD propagation. We next tested whether basal levels of Zn^{2+} present in the slices or Zn^{2+} released endogenously during SD may serve to inhibit SD propagation. Zn^{2+} levels in the extracellular space could be contributed to by multiple sources, including contamination of recording solutions (Kay 2004), or release from synaptic vesicles (Frederickson et al. 2005) and other endogenous sources (Frederickson et al. 2005; Sensi et al. 2009). Figure 2*A* shows that preexposure to a membrane-permeable Zn^{2+} chelator (TPEN; 50 μM, 10-min preexposure), significantly increased

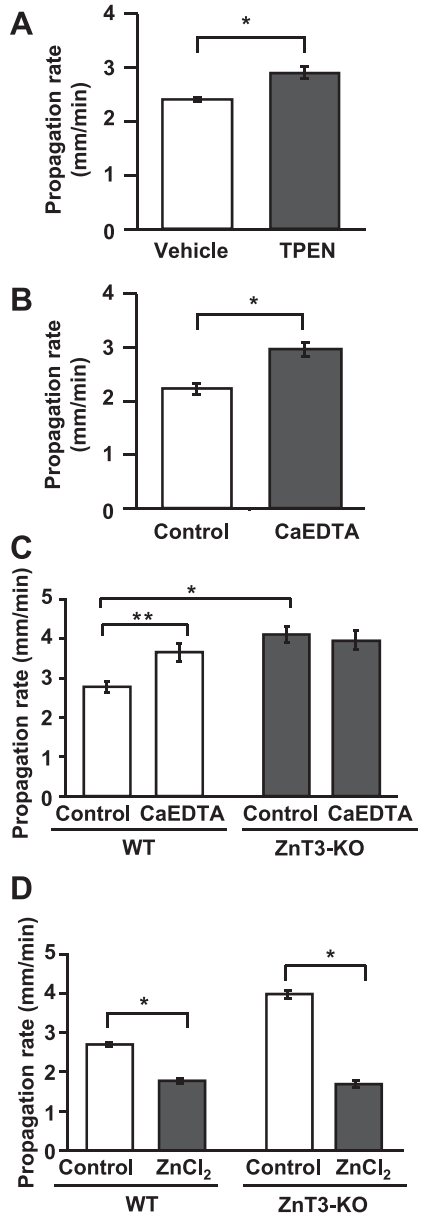

Fig. 2. SD propagation rate in wild-type (WT) and vesicular Zn^{2+} transporter ZnT-3 knockout (KO) animals in vitro. *A* and *B*: effects of Zn^{2+} chelation on SD propagation rate. Slices were preincubated with 1 of 2 Zn^{2+} chelators before SD initiation, TPEN (50 μM; *A*) or CaEDTA (1 mM; *B*). Both chelators significantly increased SD propagation rates (*$P < 0.01$; $n = 5$). *C*: in slices from ZnT-3 KO animals (filled bars), control SD propagation rates were significantly higher than those observed in WT slices. In addition, Zn^{2+} chelation with CaEDTA did not further increase SD propagation rates in ZnT-3 KO slices (*$P < 0.01$, **$P < 0.05$; $n = 5$). *D*: $ZnCl_2$ (100 μM, 10 min) effectively decreased SD propagation rate in both WT and ZnT-3 KO preparation. Experiments were interleaved between WT and ZnT-3 KO (*$P < 0.01$; $n = 5$).

SD propagation rate. In a second different set of preparations, slices were preexposed to CaEDTA (1 mM), a Zn^{2+} chelator with poor membrane permeability. CaEDTA exposures were kept short (10 min) to minimize potential depletion of intracellular Zn^{2+} pools (Frederickson et al. 2002). Under these conditions, CaEDTA also significantly increased rate of SD propagation (Fig. 2*B*). These results suggest that extracellular Zn^{2+} that is present within slices inhibits SD propagation rate.

Zn^{2+} is highly enriched in glutamatergic synaptic vesicles and is released at high levels during SD at the propagating wave front (Carter et al. 2011). To evaluate a possible contribution of this source of endogenous Zn^{2+} to inhibition of SD propagation, we compared SD propagation rates in brain slices from WT and ZnT-3 KO animals. ZnT-3 is a vesicular Zn^{2+} transporter, and thus genetic deletion of ZnT-3 results in loss of synaptic Zn^{2+} (Cole et al. 1999) and abolished extracellular accumulation of Zn^{2+} following SD (Carter et al. 2011). As shown in Fig. 2*C*, ZnT-3 KO preparations showed significantly faster SD propagation rates than those in WT preparations (WT: 2.78 ± 0.15 mm/min, ZnT-3 KO: 4.12 ± 0.47 mm/min; $P < 0.001$; $n = 5$). In addition, unlike WT preparations, pretreatment with the Zn^{2+} chelator CaEDTA did not increase propagation rates in ZnT-3 KO slices.

In a different set of experiments, the effects of exogenous $ZnCl_2$ applications were also compared between WT and ZnT-3 KO slices. As shown in Fig. 2*D*, $ZnCl_2$ (100 μM) decreased SD propagation rates in both WT and ZnT-3 KO preparations to a similar degree. These data support the idea that higher propagation rates in ZnT-3 KO are likely due to lack of vesicular Zn^{2+} release and action rather than changes in Zn^{2+} sensitivity.

Together, these results suggest that Zn^{2+} released from synaptic vesicles during SD inhibits propagation of the advancing SD wave front.

Vesicular Zn^{2+} inhibits CSD propagation in vivo. We next tested the significance of the in vitro results for CSD in vivo. Electrical recordings were made from the parietal cortex of anesthetized mice, and CSD was generated by stimulation of the cortical surface in an anterior cranial window by using either a bipolar stimulating electrode or repetitive KCl applications (see MATERIALS AND METHODS; Fig. 3*A*). Figure 3*B* shows a representative CSD generated by electrical stimulation in a WT animal. The *top* shows a characteristic DC deflection that lasts for ~1 min. This was accompanied by a longer-lasting (~5-min) depression of ECoG activity (Fig. 3*B*, *middle* and *bottom*).

CSD was reliably generated by both electrical and KCl stimuli in all WT and ZnT-3 KO animals studied, with no differences in electrical properties of single CSD episodes. Figure 3, *C* and *D*, compares the amplitudes and durations of DC deflections in both genotypes, generated by electrical stimuli. No differences were observed in any of these parameters. The durations of ECoG depression were analyzed from the recovery of the power of band-passed ECoG activity (Fig. 3*B*, *middle*). We did not observe any significant difference in the depression period (50% recovery) of ECoG following CSD (Fig. 3*E*).

Figure 4*A* shows representative CSDs generated by repetitive KCl applications. CSD propagation rates were significantly faster in ZnT-3 KO animals compared with WT controls (Fig. 5*B*; WT and ZnT-3 KO, 2.38 ± 0.21 and 3.08 ± 0.22 mm/min, respectively; $P = 0.045$; $n = 6$). In addition, ZnT-3 KO animals showed markedly higher CSD frequencies than

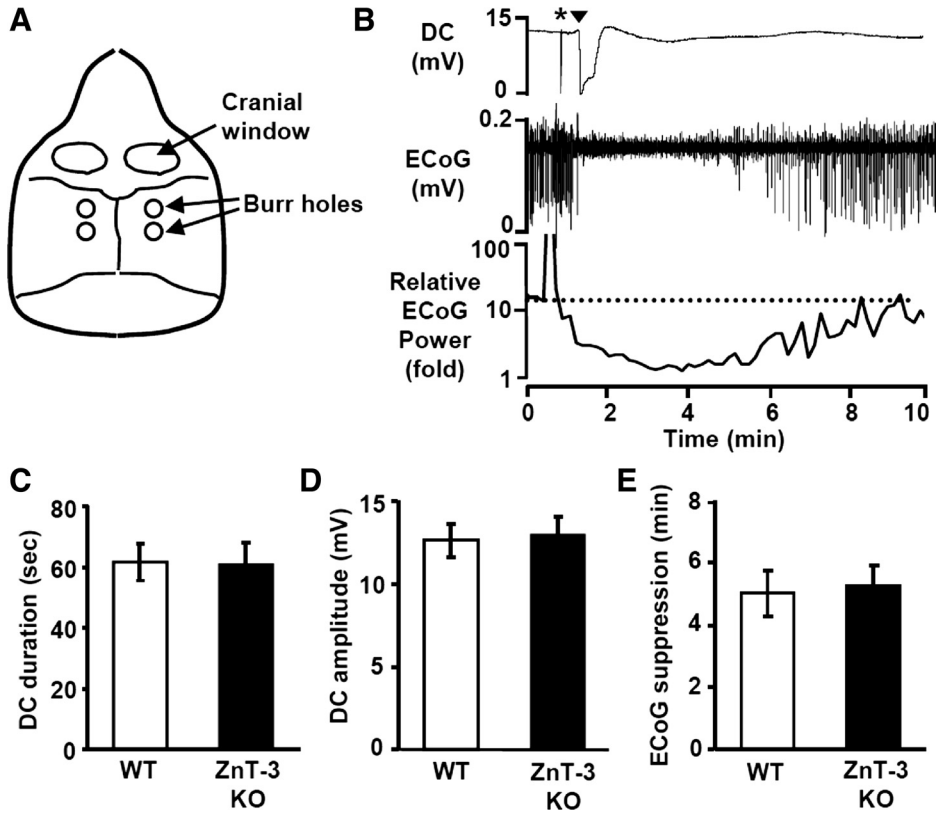

Fig. 3. Cortical spreading depression (CSD) threshold and propagation rate in WT and ZnT-3 KO animals. *A*: arrangement of craniotomies and burr holes for CSD recording. *B*: representative responses showing extracellular DC recording (*top*) and electrocorticographic (ECoG; *middle*) and relative ECoG (*bottom*; 10-s bins) power following a single CSD generated by electrical stimulation. CSD was recorded as large, long-lasting negative DC potential shift coupled with transient suppression of ECoG activity. Asterisk indicates electrical stimulation artifact. Arrowhead indicates CSD onset. *C–E*: lack of difference in the DC shift duration (*C*), DC shift amplitude (*D*), or duration of ECoG suppression (*E*; measured as 50% recovery time). $n = 6$ For each.

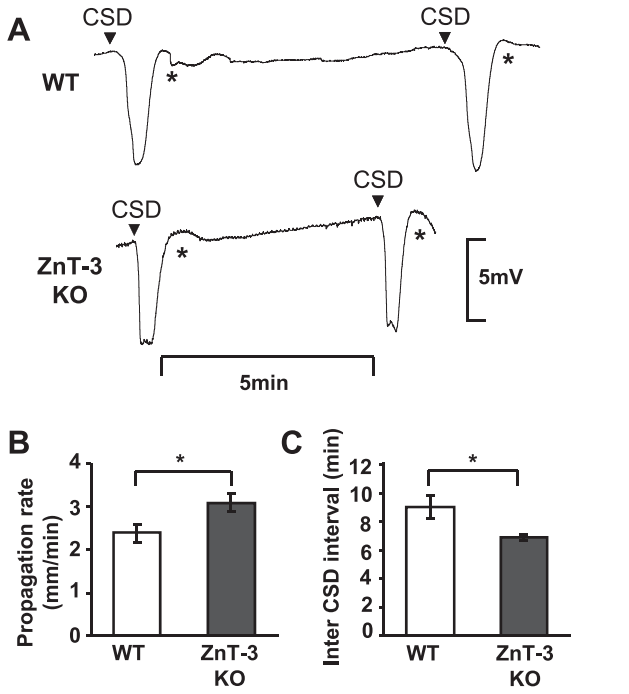

Fig. 4. ZnT-3 KO animals showed higher CSD incidence. Increased CSD propagation rates and frequencies in ZnT-3 KO animals. *A*: representative traces of repetitive CSD generated by topical KCl applications in WT and ZnT-3 KO. Arrowheads indicate onset of CSD, and recording artifacts generated by reapplication of KCl are denoted by asterisks. *B*: propagation rates of CSD in WT and ZnT-3 KO. Mean SD propagation rates were determined for each animal from the time offset between CSDs detected with a pair of electrodes. (*$P < 0.05$; $n = 6$.) *C*: inter-CSD intervals were significantly lower of ZnT-3 KO animals. (*$P < 0.001$; $n = 6$.)

WT animals (Fig. 4*C*). Thus ZnT-3 KO animals showed significantly higher numbers of CSDs in a 30-min recording period (WT and ZnT-3 KO, 3.3 ± 0.28 and 4.2 ± 0.33, respectively; $P = 0.011$; $n = 6$), associated with shorter inter-SD intervals (Fig. 4*C*; WT and ZnT-3 KO, 9.5 ± 1.4 min and 6.9 ± 0.5 min, respectively; $P = 0.0053$; $n = 6$). In normal brain, ECoG suppression is usually significantly shorter than the duration of the inter-SD interval, and thus CSDs rarely invade at-risk tissue where ECoG is still suppressed. However, in ZnT-3 KO animals, the significant decrease in inter-SD interval [without a concomitant decrease in ECoG suppression duration (compare Figs. 4*C* and 3*E*)] increased the incidence of CSD propagating into ECoG-suppressed brain. This observation suggests that extracellular Zn^{2+} could play a role in preventing CSD propagation into the unrecovered brain tissue (see DISCUSSION). These results are consistent with the hypothesis that synaptic Zn^{2+} release inhibits CSD propagation rate and frequency in vivo.

Potential extracellular Zn^{2+} targets that could contribute to modulation of SD propagation. As described above (Introduction), NMDA-Rs are a candidate target to explain the inhibitory effect of extracellular Zn^{2+} on SD propagation. Previous work has shown that $ZnCl_2$ inhibits NMDA-R at the hippocampal CA1 synapse (Izumi et al. 2006; Vogt et al. 2000), and Fig. 5, *A* and *B*, confirms that $ZnCl_2$ concentration-dependently decreased isolated $fEPSP_{NMDA}$ evoked by single stimuli (see MATERIALS AND METHODS). Comparing Figs. 1*C* and 5*B* shows that $ZnCl_2$ was more effective against $fEPSP_{NMDA}$ than against SD propagation. Figure 5, *C–E*, demonstrates that a similar mismatch in effectiveness was also observed with the synthetic NMDA-R antagonist D-AP5. Thus low concentrations of D-AP5 (2–20 μM) readily inhibit or block $fEPSP_{NMDA}$ (Fig. 5, *C* and *D*), whereas higher concentrations are required either to slow SD propagation (20–50 μM) or block the response completely (100 μM, $n = 4$). A mismatch in sensitivity to NMDA-R antagonism could be due to much higher levels of extracellular glutamate accumulating during SD compared with EPSPs generated by single electrical stimuli. Different pools of NMDA-R (different subunit composition and/or synaptic/extrasynaptic localization) activated in these different responses could also contribute (see DISCUSSION).

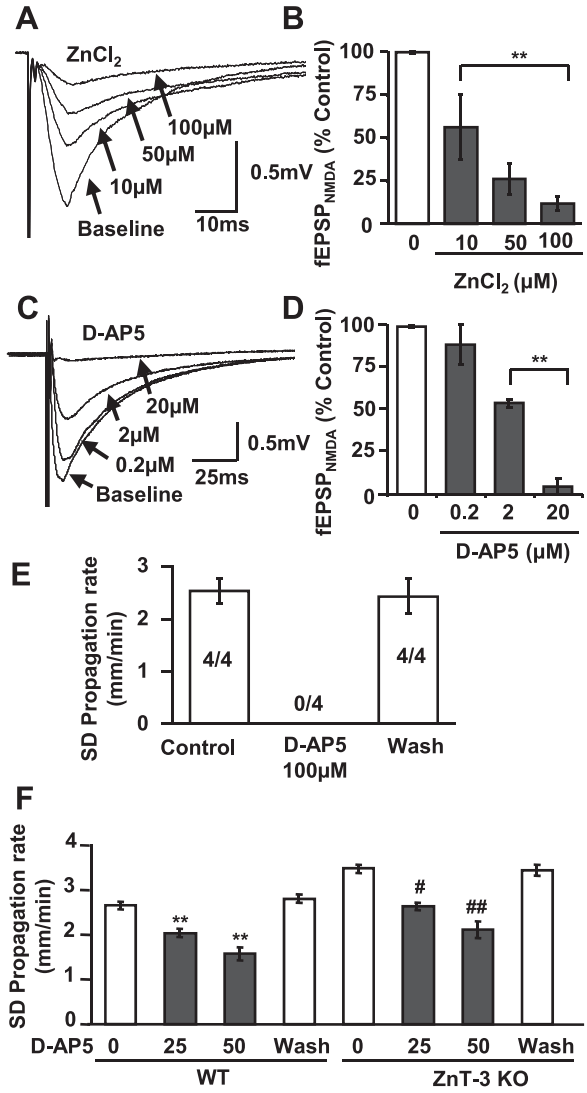

Fig. 5. Partial inhibition of *N*-methyl-D-aspartate (NMDA) receptor (NMDA-R) could contribute to effects of $ZnCl_2$ on SD propagation rate. *A* and *B*: $ZnCl_2$ partially inhibits NMDA-R. Isolated NMDA-R components of evoked field excitatory postsynaptic potential (fEPSP; see MATERIALS AND METHODS) were reduced by $ZnCl_2$ in a concentration-dependent manner (10–100 μM, 10 min). *C–F*: partial inhibition of NMDA-R with synthetic antagonist D-AP5 inhibits SD propagation. *C* and *D* show concentration-dependent inhibition of $fEPSP_{NMDA}$ (**$P < 0.01$; $n = 3$). *E* shows that D-AP5 at 100 μM reversibly abolished SD. The proportion of preparations demonstrating SD is indicated by the numbers in the bars. *F* shows that D-AP5 reversibly decreased SD propagation rates in both WT and ZnT-3 KO preparations. Recovery was evaluated after at least 30-min washout of D-AP5 (**$P < 0.01$ vs. WT control, #$P < 0.05$, ##$P < 0.01$ vs. ZnT-3 KO control; $n = 5$).

The similarity between effects of D-AP5 and $ZnCl_2$ on $fEPSP_{NMDA}$ and SD inhibition is consistent with a role for NMDA-R in the actions of Zn^{2+} to inhibit SD propagation but does not provide a direct test of the hypothesis. One approach would be to block fully NMDA-Rs involved in SD with D-AP5 and then determine whether $ZnCl_2$ lost the ability to slow the event. However, because high concentrations of D-AP5 completely prevented initiation and propagation of SD (Fig. 5*E*), this type of test was not possible. Figure 5*F* shows a different study where inhibitory effects of endogenous Zn^{2+} were removed by using the ZnT-3 KO and then the effectiveness of AP-5 was tested. In this case, baseline SD propagation rates were elevated by synaptic Zn^{2+} removal (as in Fig. 2*C*), but D-AP5 retained the same degree of block as was observed in WT tissues (WT vs. control: 22.9 ± 0.04 vs. 23.9 ± 0.02% inhibition with 25 μM D-AP5; 40.9 ± 0.05 vs. 39.5 ± 0.04% for 50 μM D-AP5). This suggests that there was no significant cooperativity between Zn^{2+} and D-AP5 in inhibiting SD, and this could be due to either different sites of action of these inhibitors on the NMDA-R (Paoletti and Neyton 2007) and/or because Zn^{2+} interacts with other extracellular targets to reduce excitability and inhibit SD.

Figure 6 shows that incubation with $ZnCl_2$ (100 μM) did not result in significant changes in resting potential, action potential number, or input resistance of single CA1 pyramidal neurons (Fig. 6, *A–D*). Furthermore, consistent with a previous report (Izumi et al. 2006), $ZnCl_2$ had no significant effect on a measure of presynaptic release probability − paired-pulse ratio (PPR) of evoked fEPSPs (Fig. 6, *E* and *F*; $P > 0.5$; $n = 4$). $ZnCl_2$ also had no effect the amplitudes of evoked fEPSPs (100 μM $ZnCl_2$: 98.5 ± 13% of control; $P > 0.1$; $n = 4$). Similarly, no significant difference in the evoked responses between WT and ZnT-3 KO preparations were observed [input-output curve (range: 0.2–0.6 mA), PPR (interpulse interval: 20, 50, and 100 ms); $P > 0.1$ in both tests; $n = 5$]. These data imply that there was no significant Zn^{2+} inhibition of evoked presynaptic Ca^{2+} influx and glutamate release or of DL-α-amino-3-hydroxy-5-methylisoxazole-propionic acid (AMPA) receptors that might contribute to decreased SD propagation rates (Kunkler and Kraig 2004; Pietrobon 2010).

Figure 6*G* shows that $GABA_A$-R activation contributes significantly to limiting the rate of SD, since full block of these channels with gabazine significantly enhanced SD propagation rate. Since $GABA_A$-Rs are known to be inhibited by Zn^{2+} (Frederickson et al. 2005; Sensi et al. 2009; Weiss et al. 2000), actions on these channels cannot be directly responsible for inhibitory effects of SD on propagation rate. Furthermore, when $GABA_A$-Rs were fully blocked with gabazine, $ZnCl_2$ was not more effective than in control conditions (mean inhibitory effect of $ZnCl_2$; control 28.9%, gabazine 29.3%; Fig. 6*G*; $*P < 0.01$).

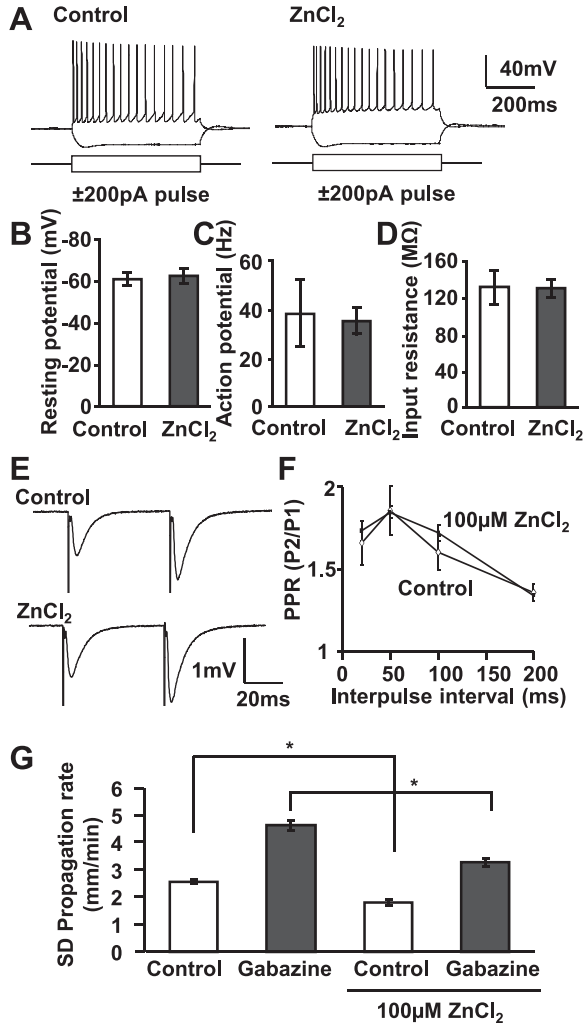

Fig. 6. Lack of effect on intrinsic excitability, presynaptic release or $GABA_A$-R mechanisms. *A–D*: lack of effect on intrinsic excitability of CA1 pyramidal neurons tested by recording responses to intracellular current injection (representative traces in *A*). $ZnCl_2$ (100 μM, 10–30 min, $n = 8$ each) had no effect on resting potential (*B*), action potential frequency (*C*), or input resistance (*D*). *E* and *F*: no significant effect of $ZnCl_2$ (100 μM, 10 min) on paired-pulse ratios (PPR) of fEPSPs as determined from the ratio of the 2nd pulse (P2) to the 1st pluse (P1) ($P = 0.50$; $n = 4$). *G*: $GABA_A$-R block by gabazine (10 μM) significantly increased SD propagation rate. The degree of SD acceleration by gabazine was unaffected by $ZnCl_2$ (100 μM, 10 min; $*P < 0.01$; $n = 4$).

DISCUSSION

General. The current study demonstrates that Zn^{2+} released during SD can serve to limit progression of the event. This conclusion is supported by consequences of exogenous Zn^{2+} applications, increased SD propagation rates following extracellular Zn^{2+} chelation, and higher SD propagation rates in ZnT-3 KO preparations. The significance of results in brain slices was confirmed in an in vivo CSD model in which ZnT-3 KO animals had higher CSD propagation rates and frequencies than WT animals. Previous work has emphasized a neurotoxic role of intracellular Zn^{2+} accumulation (Sensi et al. 2009; Weiss et al. 2000). However, our current study raises the possibility that the synaptic Zn^{2+} released during SD may be beneficial in some contexts by limiting SD.

Zn^{2+} released from synaptic vesicles inhibits SD propagation. Zn^{2+} is capable of interacting with a large number of ion channels, receptors, and intracellular signaling pathways (Frederickson et al. 2005; Sensi et al. 2009; Weiss et al. 2000), however, the inhibitory actions of Zn^{2+} on SD propagation appear to be due to extracellular actions rather than intracellular accumulation. Thus selective approaches to increase intracellular Zn^{2+} (with zinc pyrithione) did not retard SD, and the inhibitory effects of brief $ZnCl_2$ exposures were readily

reversible. Both of these observations are compatible with interaction of an extracellular target.

The fact that brief exposures to Zn^{2+}-selective chelators significantly increased SD propagation rates implies that there is sufficient extracellular Zn^{2+} within the slice to inhibit SD propagation. Two main sources of Zn^{2+} need to be considered: contamination of Zn^{2+} from a variety of exogenous sources (Kay 2004) and endogenous sources including synaptic vesicles. Results from tissues lacking Zn^{2+} in synaptic vesicles (ZnT-3 KO) show that release from vesicles underlies these effects. Thus SD generated in ZnT-3 KO preparations was significantly faster than in WT tissues, both measured in vitro in hippocampal slices and in vivo during CSD. Importantly, the potentiating effects of CaEDTA were abolished in ZnT-3 KO slices, demonstrating no additional effect of contaminating Zn^{2+}.

We recently showed that a large release of Zn^{2+} from synaptic vesicles accompanies the advancing SD wave front (Carter et al. 2011), and it seems likely that such release is responsible for retarding progression of the event. If this is the case, then release should occur just before the complete depolarization that characterizes SD. It is noted that SD propagation is preceded by an episodic transient hyperexcitation (Herreras et al. 1994; Larrosa et al. 2006), which is associated with increase of spontaneous EPSC frequencies (Aiba I and Shuttleworth CW, unpublished observations). The exact extracellular Zn^{2+} concentrations achieved during and after SD are not yet clear. However, extracellular Zn^{2+} transients generated by SD were ~10 times higher than those produced by trains of electrical stimulation, and from comparison with prior work (Assaf and Chung 1984; Howell et al. 1984), it seems likely that Zn^{2+} concentrations can reach at least 100 μM in synaptic clefts following SD. However, estimates of extracellular Zn^{2+} concentrations are controversial and need to be consolidated (Frederickson et al. 2005; Kay 2003).

Potential mechanisms contributing to Zn^{2+} inhibition of SD. We did not observe effects of $ZnCl_2$ on intrinsic excitability or synaptic function that could explain the decrease in SD propagation rate. A marked increase in extracellular GABA concentration has been reported during SD (Molchanova et al. 2004), and Zn^{2+} can inhibit $GABA_A$-Rs (Smart et al. 2004), but based on the effects of $GABA_A$-R block with gabazine (Fig. 6), such an action of Zn^{2+} would be expected to accelerate (rather than inhibit) SD propagation.

One candidate for decreases in SD propagation is inhibition of NMDA-Rs. As described above (Introduction) and demonstrated in the present work, NMDA-R antagonists can completely abolish some forms of SD, presumably by substantially increased threshold for initiation. Activation of NMDA-R at the advancing wave front also appears to contribute significantly to setting the SD propagation rate. Previous work showed that the competitive NMDA-R antagonist CPP slowed SD propagation in brain slice (Larrosa et al. 2006), and the present study extends these observations by showing that with partial inhibition of NMDA-R, SD could still be generated but propagated substantially more slowly than in control conditions.

In the present study, we confirmed effective inhibition of NMDA-R by exogenous application of $ZnCl_2$, but it was not possible to inhibit evoked NMDA potentials completely with $ZnCl_2$. A similar partial block of NMDA-R components of fEPSPs was reported previously (Izumi et al. 2006). At least two factors could contribute to the partial nature of this block. First, Zn^{2+} preferentially inhibits NMDA-Rs containing NR2A subunits, and significantly higher concentrations are required to inhibit NR2B-containing receptors (Gielen et al. 2009; Paoletti and Neyton 2007). Zn^{2+}-sensitive NR2A-containing receptors appear more predominantly localized to synaptic sites, whereas extrasynaptic regions may express more NR2B-containing receptors (Hardingham and Bading 2010). Thus a potentially greater involvement of extrasynaptic receptors during massive glutamate release at the SD wave front might explain the weaker inhibitory effects of Zn^{2+} on SD compared with evoked synaptic potentials. Second, the effective concentration of Zn^{2+} that can be achieved in brain slice studies is limited by solubility in the ACSF-based recording solutions. Zn^{2+} interacts with and precipitate with phosphate and thus decrease activity of Zn^{2+}, and for this reason, histidine was included in recording solutions to increase availability (Rumschik et al. 2009). However, it is likely that the effects were still underestimated. Some combination of these two factors is expected to explain why SD was slowed but not abolished by the concentrations of $ZnCl_2$ we could test in this study.

The similarity between effects of D-AP5 and $ZnCl_2$ on $fEPSP_{NMDA}$ and SD inhibition is consistent with a role for NMDA-R in the actions of Zn^{2+} to inhibit SD propagation, but (as noted above in RESULTS) direct tests of this hypothesis were not possible due to the essential requirement of NMDA-R for generation of the SD event. Thus it is not yet known whether inhibition of NMDA-R might be sufficient to explain decreased SD propagation rate and/or whether other targets of Zn^{2+}, including the recently described zinc-sensing metabotropic receptor (Chorin et al. 2011), could also contribute.

Implications for Zn^{2+}-based interventions to limit brain injury. Important studies have shown that Zn^{2+} chelation can be neuroprotective in rodent stroke models, and a large body of work has identified multiple intracellular pathways linking intracellular Zn^{2+} accumulation to injury (Koh et al. 1996; Sensi et al. 2009; Sheline et al. 2000; Weiss et al. 2000). However, on the other hand, several studies have suggested opposite (neuroprotective) roles of Zn^{2+} in ischemic injury (Galasso and Dyck 2007). Thus administration of exogenous Zn^{2+} decreased ischemic lesion size (Zhao et al. 1996), and pretreatment with CaEDTA has been shown to accelerate early ischemic infarct formation in a rat stroke model (Kitamura et al. 2006). In addition, ZnT-3 KO animals have been shown to have higher susceptibility to some other forms of brain injury (Cole et al. 2000; Doering et al. 2010).

Recent work has consolidated the idea that SD can contribute significantly to the expansion of ischemic injuries (Dreier 2011; Lauritzen et al. 2011), and it is possible that divergent effects of Zn^{2+} on SD explains the apparently contradictory effects of Zn^{2+} chelation in different injury models. Thus we recently provided evidence that Zn^{2+} chelation increased the threshold for initiation of some forms of SD in brain slices. This was attributed to intracellular Zn^{2+} accumulation, which likely contributed to metabolic failure in an in vitro ischemia model (Dietz et al. 2008). Substantial synaptic Zn^{2+} release also accompanies SD and leads to postsynaptic uptake (Carter et al. 2011), raising the possibility that Zn^{2+} released during repetitive SDs in ischemia can prime injured tissues by lowering SD threshold and/or activating other intracellular cell

death pathways. However, Zn^{2+} chelation did not prevent initiation of SD under normoxic conditions (Dietz et al. 2008 and present study), presumably because the initiation of these events was determined by localized accumulation of K^+ rather than progressive depletion of metabolites.

The current study reveals an additional important complexity to the actions of Zn^{2+} in SD by describing significant extracellular actions. By slowing the progression of recurrent SD events through peri-infarct regions, synaptic release of Zn^{2+} could limit the deleterious invasion of SDs into tissue that has not fully recovered from previous depolarizations. It will be of interest to determine the relationship between extracellular Zn^{2+} accumulation and the durations of DC shifts and ECoG recovery in rodent models of focal ischemia to evaluate this possibility.

The idea of opposing intracellular and extracellular actions of Zn^{2+} may emerge as a common theme in Zn^{2+} pathophysiology, as a recent report showed that although intracellular Zn^{2+} accumulation contributes to neuronal excitability due to KCC2 downregulation, binding of Zn^{2+} to an extracellular receptor leads to activation of KCC2 (Chorin et al. 2011). These considerations further strengthen the idea that strategies that specifically target intracellular Zn^{2+} accumulation (while maintaining potentially beneficial effects of extracellular Zn^{2+}) could be more effective interventions for ischemic stroke.

GRANTS

This study was supported by National Institutes of Health Grants NS-051288 (C. W. Shuttleworth) and DK-073446 (C. T. Sheline) and American Heart Association Grant 11PRE4870002 (I. Aiba).

DISCLOSURES

No conflicts of interest, financial or otherwise, are declared by the author(s).

AUTHOR CONTRIBUTIONS

I.A., C.T.S., and C.W.S. conception and design of research; I.A. and A.P.C. performed experiments; I.A. analyzed data; I.A., A.P.C., and C.W.S. interpreted results of experiments; I.A. prepared figures; I.A. and C.W.S. drafted manuscript; I.A., A.P.C., C.T.S., and C.W.S. edited and revised manuscript; I.A., A.P.C., C.T.S., and C.W.S. approved final version of manuscript.

REFERENCES

Anderson TR, Andrew RD. Spreading depression: imaging and blockade in the rat neocortical brain slice. *J Neurophysiol* 88: 2713–2725, 2002.

Assaf SY, Chung SH. Release of endogenous Zn^{2+} from brain tissue during activity. *Nature* 308: 734–736, 1984.

Carter RE, Aiba I, Dietz RM, Sheline CT, Shuttleworth CW. Spreading depression and related events are significant sources of neuronal Zn(2+) release and accumulation. *J Cereb Blood Flow Metab* 31: 1073–1084, 2011.

Chorin E, Vinograd O, Fleidervish I, Gilad D, Herrmann S, Sekler I, Aizenman E, Hershfinkel M. Upregulation of KCC2 activity by zinc-mediated neurotransmission via the mZnR/GPR39 receptor. *J Neurosci* 31: 12916–12926, 2011.

Cole TB, Robbins CA, Wenzel HJ, Schwartzkroin PA, Palmiter RD. Seizures and neuronal damage in mice lacking vesicular zinc. *Epilepsy Res* 39: 153–169, 2000.

Cole TB, Wenzel HJ, Kafer KE, Schwartzkroin PA, Palmiter RD. Elimination of zinc from synaptic vesicles in the intact mouse brain by disruption of the ZnT3 gene. *Proc Natl Acad Sci USA* 96: 1716–1721, 1999.

Dietz RM, Weiss JH, Shuttleworth CW. Zn^{2+} influx is critical for some forms of spreading depression in brain slices. *J Neurosci* 28: 8014–8024, 2008.

Doering P, Stoltenberg M, Penkowa M, Rungby J, Larsen A, Danscher G. Chemical blocking of zinc ions in CNS increases neuronal damage following traumatic brain injury (TBI) in mice. *PLoS One* 5: e10131, 2010.

Dreier JP. The role of spreading depression, spreading depolarization and spreading ischemia in neurological disease. *Nat Med* 17: 439–447, 2011.

Fabricius M, Jensen LH, Lauritzen M. Microdialysis of interstitial amino acids during spreading depression and anoxic depolarization in rat neocortex. *Brain Res* 612: 61–69, 1993.

Faria LC, Mody I. Protective effect of ifenprodil against spreading depression in the mouse entorhinal cortex. *J Neurophysiol* 92: 2610–2614, 2004.

Frederickson CJ, Koh JY, Bush AI. The neurobiology of zinc in health and disease. *Nat Rev Neurosci* 6: 449–462, 2005.

Frederickson CJ, Suh SW, Koh JY, Cha YK, Thompson RB, LaBuda CJ, Balaji RV, Cuajungco MP. Depletion of intracellular zinc from neurons by use of an extracellular chelator in vivo and in vitro. *J Histochem Cytochem* 50: 1659–1662, 2002.

Galasso SL, Dyck RH. The role of zinc in cerebral ischemia. *Mol Med* 13: 380–387, 2007.

Gielen M, Siegler Retchless B, Mony L, Johnson JW, Paoletti P. Mechanism of differential control of NMDA receptor activity by NR2 subunits. *Nature* 459: 703–707, 2009.

Gill R, Andine P, Hillered L, Persson L, Hagberg H. The effect of MK-801 on cortical spreading depression in the penumbral zone following focal ischaemia in the rat. *J Cereb Blood Flow Metab* 12: 371–379, 1992.

Hardingham GE, Bading H. Synaptic versus extrasynaptic NMDA receptor signalling: implications for neurodegenerative disorders. *Nat Rev Neurosci* 11: 682–696, 2010.

Hartings JA, Rolli ML, Lu XC, Tortella FC. Delayed secondary phase of peri-infarct depolarizations after focal cerebral ischemia: relation to infarct growth and neuroprotection. *J Neurosci* 23: 11602–11610, 2003.

Hartings JA, Watanabe T, Bullock MR, Okonkwo DO, Fabricius M, Woitzik J, Dreier JP, Puccio A, Shutter LA, Pahl C, Strong AJ. Spreading depolarizations have prolonged direct current shifts and are associated with poor outcome in brain trauma. *Brain*, 2011.

Herreras O, Largo C, Ibarz JM, Somjen GG, Martín del Río R. Role of neuronal synchronizing mechanisms in the propagation of spreading depression in the in vivo hippocampus. *J Neurosci* 14: 7087–7098, 1994.

Howell GA, Welch MG, Frederickson CJ. Stimulation-induced uptake and release of zinc in hippocampal slices. *Nature* 308: 736–738, 1984.

Izumi Y, Auberson YP, Zorumski CF. Zinc modulates bidirectional hippocampal plasticity by effects on NMDA receptors. *J Neurosci* 26: 7181–7188, 2006.

Kay AR. Detecting and minimizing zinc contamination in physiological solutions. *BMC Physiol* 4: 4, 2004.

Kay AR. Evidence for chelatable zinc in the extra cellular space of the hippocampus, but little evidence for synaptic release of Zn. *J Neurosci* 23: 6847–6855, 2003.

Kitamura Y, Iida Y, Abe J, Ueda M, Mifune M, Kasuya F, Ohta M, Igarashi K, Saito Y, Saji H. Protective effect of zinc against ischemic neuronal injury in a middle cerebral artery occlusion model. *J Pharm Sci* 100: 142–148, 2006.

Koh JY, Suh SW, Gwag BJ, He YY, Hsu CY, Choi DW. The role of zinc in selective neuronal death after transient global cerebral ischemia. *Science* 272: 1013–1016, 1996.

Kunkler PE, Kraig RP. P/Q Ca^{2+} channel blockade stops spreading depression and related pyramidal neuronal Ca^{2+} rise in hippocampal organ culture. *Hippocampus* 14: 356–367, 2004.

Larrosa B, Pastor J, Lopez-Aguado L, Herreras O. A role for glutamate and glia in the fast network oscillations preceding spreading depression. *Neuroscience* 141: 1057–1068, 2006.

Lauritzen M, Dreier JP, Fabricius M, Hartings JA, Graf R, Strong AJ. Clinical relevance of cortical spreading depression in neurological disorders: migraine, malignant stroke, subarachnoid and intracranial hemorrhage, and traumatic brain injury. *J Cereb Blood Flow Metab* 31: 17–35, 2011.

Leão AA. Spreading depression of activity in the cerebral cortex. *J Neurophysiol* 7: 359–390, 1944.

Molchanova S, Koobi P, Oja SS, Saransaari P. Interstitial concentrations of amino acids in the rat striatum during global forebrain ischemia and potassium-evoked spreading depression. *Neurochem Res* 29: 1519–1527, 2004.

Paoletti P, Ascher P, Neyton J. High-affinity zinc inhibition of NMDA NR1-NR2A receptors. *J Neurosci* 17: 5711–5725, 1997.

Paoletti P, Neyton J. NMDA receptor subunits: function and pharmacology. *Curr Opin Pharmacol* 7: 39–47, 2007.

Paoletti P, Vergnano AM, Barbour B, Casado M. Zinc at glutamatergic synapses. *Neuroscience* 158: 126–136, 2009.

Peeters M, Gunthorpe MJ, Strijbos PJ, Goldsmith P, Upton N, James MF. Effects of pan- and subtype-selective *N*-methyl-D-aspartate receptor antagonists on cortical spreading depression in the rat: therapeutic potential for migraine. *J Pharmacol Exp Ther* 321: 564–572, 2007.

Pietrobon D. Insights into migraine mechanisms and CaV2.1 calcium channel function from mouse models of familial hemiplegic migraine. *J Physiol* 588: 1871–1878, 2010.

Qian J, Noebels JL. Visualization of transmitter release with zinc fluorescence detection at the mouse hippocampal mossy fibre synapse. *J Physiol* 566: 747–758, 2005.

Rumschik SM, Nydegger I, Zhao J, Kay AR. The interplay between inorganic phosphate and amino acids determines zinc solubility in brain slices. *J Neurochem* 108: 1300–1308, 2009.

Sensi SL, Paoletti P, Bush AI, Sekler I. Zinc in the physiology and pathology of the CNS. *Nat Rev Neurosci* 10: 780–791, 2009.

Sheline CT, Behrens MM, Choi DW. Zinc-induced cortical neuronal death: contribution of energy failure attributable to loss of NAD(+) and inhibition of glycolysis. *J Neurosci* 20: 3139–3146, 2000.

Smart TG, Hosie AM, Miller PS. Zn^{2+} ions: modulators of excitatory and inhibitory synaptic activity. *Neuroscientist* 10: 432–442, 2004.

Somjen GG. Mechanisms of spreading depression and hypoxic spreading depression-like depolarization. *Physiol Rev* 81: 1065–1096, 2001.

Vander Jagt TA, Connor JA, Weiss JH, Shuttleworth CW. Intracellular Zn^{2+} increases contribute to the progression of excitotoxic Ca^{2+} increases in apical dendrites of CA1 pyramidal neurons. *Neuroscience* 159: 104–114, 2009.

Vogt K, Mellor J, Tong G, Nicoll R. The actions of synaptically released zinc at hippocampal mossy fiber synapses. *Neuron* 26: 187–196, 2000.

Weiss JH, Sensi SL, Koh JY. Zn(2+): a novel ionic mediator of neural injury in brain disease. *Trends Pharmacol Sci* 21: 395–401, 2000.

Zhao YJ, Yang GY, Domino EF. Zinc protoporphyrin, zinc ion, and protoporphyrin reduce focal cerebral ischemia. *Stroke* 27: 2299–2303, 1996.